Electronic Supplementary Material (ESI) for Chemical Communications.

Supplementary information

Graphene cladded cobalt phosphide nanoparticles with sandwich structure by low temperature plasma for lithium and sodium storage

Experimental:

Synthesis of GO

GO was prepared according to the methods reported in the literature. First, 5g graphite, 2.5g $NaNO_3$ dissolved in 120 mL H_2SO_4 (95%). The obtained solution was slowly mixed with 15g KMnO4 under rapid magnetic stirring. Next, the mixed solution was aged at room temperature for 24 h. Dilute with 150ml ultra-pure water and continue stirring for 48h. Then 50ml H_2O_2 (30%) was added, and the mixture was washed with water for several times. Finally, the mixture is dried to GO.

Synthesis of the precursor

Dissolve 0.05 g cobalt nitrate hexahydrate, 0.03 g ammonium fluoride and 0.1 g urea in 20 ml deionized water and stir well on a magnetic stirrer. 50 mg GO was dissolved in 30 ml deionized water and stirred by ultrasonic to form a uniform GO suspension. The mixture was then poured into a blue-mouthed bottle and bathed in oil at 90℃ for 20 h. After the oil bath reaction was completed, the samples were cooled to room temperature and cleaned with deionized water for several times. After 48 hours freeze-drying, black cotton batting samples were collected.

Synthesis of CoP@RGO by low temperature plasma phosphating method

The phosphating furnace is Plasma Enhanced Chemical Vapor Deposition (PECVD). As shown in Figure.1a, red phosphorus and precursor were placed upstream and downstream of the quartz tube, respectively. First, the furnace is vacuumed to less than 5 Pa. Then, Ar/H_2 mixture gas fills into the chamber. After the airflow stabilizes, turn on the power. The temperature was set at 300℃, and the time was 2 h. When the temperature reaches 300 ℃, turn on the plasma with 300 W. After phosphating, the product is cooled to room temperature under the protection of Ar atmosphere.

Synthesis of parallel samples

CoP samples were prepared in accordance with the process of CoP@GRO without GO. The CoP/RGO sample is prepared by mechanically mixing the prepared CoP sample with the commercial RGO.

Material characterization

The crystallographic structure was determined by Rigaku Ultima IV X-ray diffraction (XRD) equipped with Cu Kα radiation (λ = ~1.54178 Å). The morphology and structure of samples were characterized using a JSM 7800F field-emission scanning electron microscope and a JEM-2100

Plus transmission electron microscope with an EDS probe. Thermogravimetric analysis (TGA) was performed on a TGA-2 thermogravimetric analyzer under an Ar atmosphere up to 800 °C. PHI5000 Versaprobe III X-ray photoelectron spectrometer (XPS) measurements were used to analyzed the surface chemical states, which examined with a monochromatic Al Ka (1486.8 eV) radiation.
The inVia was used to test the Raman spectrum with laser excitation at 532 nm.

Electrochemical measurements

For anode electrodes were prepared by coating a homogenously mixed a slurry of active material, acetylene black and PVDF binder in N-methyl pyrrolidinone (NMP) with a mass ratio of 7:2:1 onto Cu foil. All the working electrodes were dried in a vacuum oven at 120 ℃ for 12 h, and the loading mass of active materials was about ~0.24 mg. $LiPF_6$/EC+DEC+EMC was selected as the electrolyte for lithium-ion batteries. $NaClO_4$ (1 M) solution in a mixture of ethylene carbonate and dimethyl carbonate (1:1 by volume) was employed as the electrolyte for sodium ion batteries.

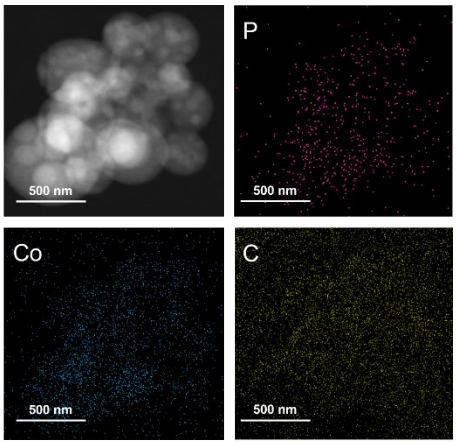

Figure S1. EDS element distribution map of P, Co, O and C.

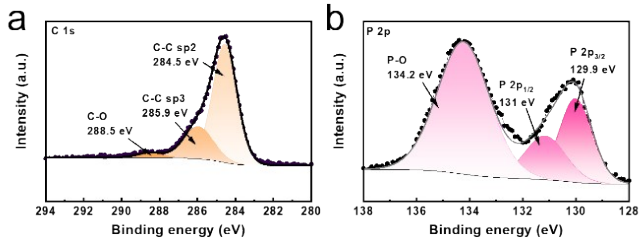

Figure S2. XPS of CoP/RGO: (a) C 1s, (b) P 2p.

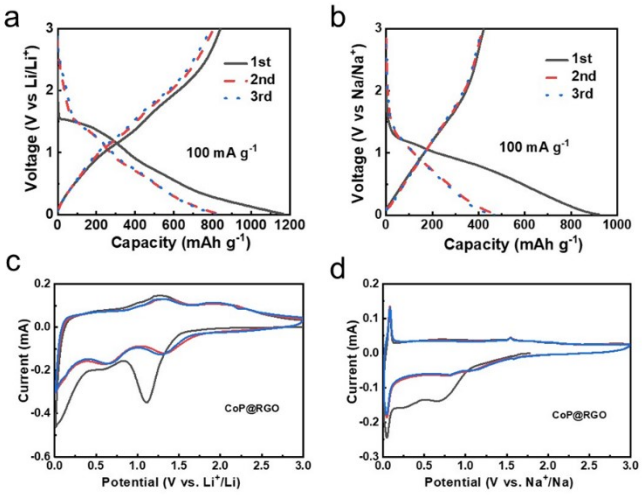

Figure S3. The first three charge-discharge curves of CoP@RGO for (a) lithium-battery and (b) sodium-battery. CV curves of CoP@RGO for the anode of (c) lithium-battery and (d) sodium-battery at scan rate of 0.2 mV s^{-1}.

The first coulomb efficiency of CoP@RGO as the anode of lithium ion batteries and sodium ion batteries are 72% and 45.7% respectively. The low ICE is caused by the formation of the SEI film in the first cycle and the irreversible binding of Li+/Na+ with defects in the RGO material.

For lithium anode, the reduction peak appearing at 1.1 V in the first cathodic scan CV curve is generated by the formation of solid electrolyte interface (SEI) film. In the second circuit of discharge, the lithiation peak at about 1.2 V corresponds to the lithiation of CoP and intermediate

Li_xCoP, and the reduction peak at about 0.6 V is related to the conversion reaction of Li_xCoP to Co^0 and Li_3P. In the charging process, the oxidation peak located at 1.1V is caused by the reaction of CoP formed by the structural reconstruction of the active substance.

When CoP@RGO is used as an anode for sodium battery, the reduction peak in the voltage range of 0.9 ~ 0.5 V in the first cathodic scan corresponds to the formation of SEI and some irreversible conversions. Reduction peak at 0.2V is caused by the formation of Na_3P. Oxidation peak at about 1.5V is typical of the gradual decomposition of Na_3P into Na_xP intermediates. In subsequent cycles, due to structural recombination, two main cathode peaks appear at 0.8V and 1V, respectively.

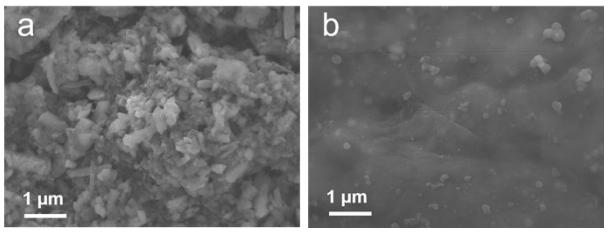

Figure S4. Morphology of anode materials in sodium ion battery after 100 cycles at 100 mA g^{-1}, (a) CoP, (b) CoP@RGO.

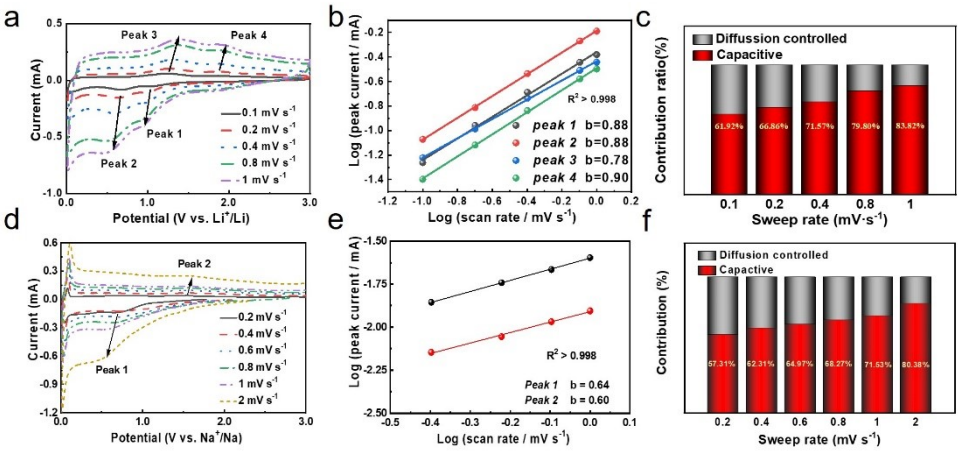

Figure S5. (a) CV curve of CoP@RGO as the anode of a lithium-ion battery (Scan rate increased from 0.1 mV s^{-1} to 1 mV s^{-1}), (b) Plots of linear fit of log(i) and log(v), (c) Capacitance contribution at different scan rates. (d) CV curve of CoP@RGO as the anode of a sodium-ion battery (Scan rate increased from 0.2 mV s^{-1} to 2 mV s^{-1}), (e) Plots of linear fit of log(i) and log(v), (f) Capacitance contribution at different scan rates.

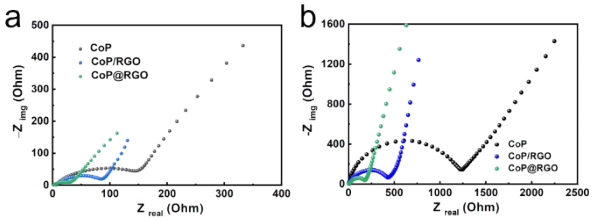

Figure S6. EIS curves of CoP, CoP/RGO and CoP@RGO as the anode of a) lithium-ion battery and

b) sodium-ion battery

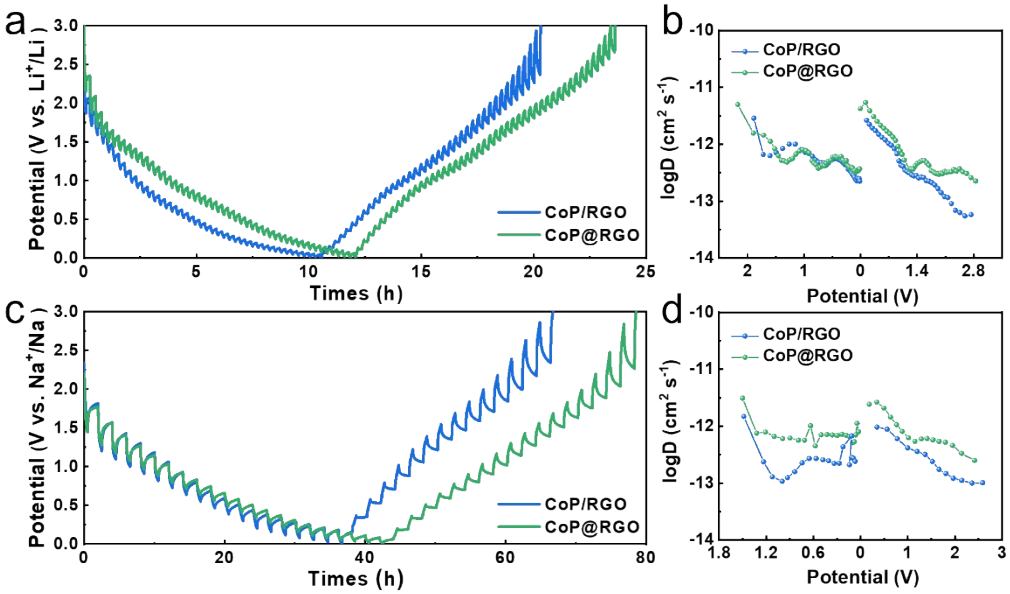

Figure S7. GITT curves of CoP@RGO as the anode of a) lithium-ion battery and c) sodium-ion battery, Plot of diffusion coefficient calculated from GITT profiles for LIBs b) and SIBs d). The calculated diffusion coefficients (D) are calculated according to GITT profiles. For lithium ion storage, the diffusion coefficients of CoP@RGO are similar to that of CoP/RGO during lithiation, but higher than that of CoP/RGO during delithification process. Significantly, during the sodiation/desodiation process, the dynamic advantages of CoP@RGO are more pronounced (Fig.S7d).

Table S1 Comparison of electrochemical performance of reported anode in LIB

Sample	**LIB Cycle performance**	**Ref.**
This work	805 mAh g^{-1} at 100 mA g^{-1} after 100cycles	
This work	685 mAh g^{-1} at 1 A g^{-1} after 500 cycles	
CoP-C@MoS_2/C	613 mAh g^{-1} at 1 A g^{-1} after 1000 cycles	1
NCP@G	1118.6 mA h g^{-1} at 0.1 A g^{-1} after 350 cycles	2
CoP-NC@$Ti_3C_2T_x$	212.9 mAh g^{-1} at 1 A g^{-1} after 2000 cycles	3
MOFs-CoP@MXene	706.5 mAh g^{-1} at 200 mA g^{-1} after 200 cycles	4
CoP/RGO	967 mA·h·g^{-1} at 200 mA g^{-1} over 200 cycles	5
CoP NFs	481.7 mA h g^{-1} at 200 mA g^{-1} after 240 cycles	6
CoP@NC/GO	506 mA h g^{-1} at 600 mA g^{-1} after 500 cycles	7
CoP⊂NPPCS	640 mAh g^{-1} at 200 mA g^{-1} after 200 cycles	8

Table S2 Comparison of electrochemical performance of reported anode in SIB

Sample	**SIB Cycle performance**	**Ref.**
This work	347 mAh g^{-1} at 100 mA g^{-1} after 100 cycles	

This work	280 mAh g^{-1} at 1 A g^{-1} after 1000 cycles	
NP-PC/CoP-2	345 mAh $\cdot g^{-1}$ at 200 mA g^{-1} after 60 cycles	[9]
Ni-CoP@CN⊂CF	312.3 mAh $\cdot g^{-1}$ at 200 mA g^{-1} over 300 cycles	[10]
H-CoP@NC	209.9 mA h g^{-1} at 2 A g^{-1} after 1000 cycles	[11]
CoP/HNC	304 mA h g^{-1} at 100 mA g^{-1} after 100 cycles	[12]
CoP/CS-800	0.834 mA h cm^{-2} at 0.2 mA cm^{-2} after 50 cycles	[13]
CoP	210 mA·h·g^{-1} at 100 mA g^{-1} at initial cycle	[14]
CoP@C-600	320 mA·h·g^{-1} at 100 mA g^{-1} after 300 cycles	[15]
CoP@C-RGO-NF	473.1 mA h g^{-1} at 100 mA g^{-1} after 100 cycles	[16]

Reference

1. Y. Xia, T. Yang, Z. Wang, T. Mao, Z. Hong, J. Han, D. L. Peng and G. Yue, *Advanced Functional Materials*, 2023, 2302830.
2. H. Zhou, Y. Zhao, Y. Jin, Q. Fan, Y. Dong and Q. Kuang, *Journal of Power Sources*, 2023, **560**, 232715.
3. X. Liu, F. Liu, X. Zhao and L.-Z. Fan, *Journal of Materiomics*, 2022, **8**, 30-37.
4. H. Zong, L. Hu, Z. Wang, R. Qi, K. Yu and Z. Zhu, *Chemical Engineering Journal*, 2021, **416**, 129102.
5. J. Yang, Y. Zhang, C. Sun, H. Liu, L. Li, W. Si, Q. Yan and X. Dong, *Nano Research*, 2016, **9**, 612-621.
6. J. Ye, F. Ge, G. Xia, Z. Zheng and C. Hu, *Materials Letters*, 2021, **282**, 128687.
7. S. Sun, T. Xie, S. Tao, P. Sheng, Z. Han, B. Qian and X. Jiang, *Energy Technology*, 2019, **8**, 1901089.
8. J. Bai, B. Xi, H. Mao, Y. Lin, X. Ma, J. Feng and S. Xiong, *Advanced Materials*, 2018, **30**, 1802310.
9. S. Liu, W. Zhang, L. Ren, Y. Li, J. Wang and C. Wang, *Chemical Engineering Science*, 2023, **280**, 119089.
10. H. Li, X. Wang, Z. Zhao, R. Pathak, S. Hao, X. Qiu and Q. Qiao, *Journal of Materials Science & Technology*, 2022, **99**, 184-192.
11. Z. Lin, X. Tan, L. Ge, Y. Lin, W. Yang, J. Lin, H. Fu, S. Ying and Z. Huang, *Journal of Alloys and Compounds*, 2022, **921**, 166075.
12. W. Huang, H. Shangguan, X. Zheng, C. Engelbrekt, Y. Yang, S. Li, K. Mølhave, X. Xiao, X. Lin, L. Ci and P. Si, *Electrochimica Acta*, 2021, **395**, 139112.
13. H. Sun, J. Wang, W. Li, F. Yuan, Q. Wang, D. Zhang, B. Wang and Y. A. Wu, *Electrochimica Acta*, 2021, **388**, 138628.
14. A. S. Murali, D. S. Baji, S. Nair and D. Santhanagopalan, *Electrochimica Acta*, 2021, **388**, 138643.
15. Q. Liu, Z. Hu, Y. Liang, L. Li, C. Zou, H. Jin, S. Wang, H. Lu, Q. Gu, S.-L. Chou, Y. Liu and S.-X. Dou, *Angew Chem Int Ed Engl*, 2020, **59**, 5159-5164.
16. X. Ge, Z. Li and L. Yin, *Nano Energy*, 2017, **32**, 117-124.